EasyChair Preprint

№ 7436

Seismic Fragility Functions of Bridge Pylons: Effects of Rayleigh-Surface Waves

Carolina Franco, Yaël Perraud and Charisis T Chatzigogos

February 7, 2022

3rd EUROPEAN CONFERENCE ON
EARTHQUAKE ENGINEERING & SEISMOLOGY
BUCHAREST, ROMANIA, 2022

Seismic Fragility Functions of Bridge Pylons: Effects of Rayleigh-surface waves

Franco Carolina - Géodynamique Structure, Immeuble Cap Sud, 106 Avenue Marx Dormoy, 92120 Montrouge, France, carolina.franco@geodynamique.com

Perraud Yaël - Géodynamique Structure, Immeuble Cap Sud, 106 Avenue Marx Dormoy, 92120 Montrouge, France, yael.perraud@geodynamique.com

Chatzigogos Charisis T - Géodynamique Structure, Immeuble Cap Sud, 106 Avenue Marx Dormoy, 92120 Montrouge, France, charisis.chatzigogos@geodynamique.com

Abstract: The quantification of the effects of surface waves on the seismic vulnerability of structures becomes relevant, especially in sedimentary basins, which tend to generate or amplify surface wave components carried by the seismic signals. Long-period large-scale infrastructures (e.g., high-rise buildings, bridges, liquid storage tanks) located on sedimentary basins may experience amplified seismic motions due to significant surface-wave content characterized by long periods and long durations. This work proposes a strategy to quantify the effects of Rayleigh waves on seismic vulnerability assessment of bridge pylons by calculating analytical fragility curves as a function of peak ground velocity (PGV). The fragility curves of bridge pylons are obtained based on nonlinear incremental dynamic analyses on several simplified pylon mechanical models. The nonlinear analyses use a set of seismic records, in which the surface wave component can be considered or not, to quantify the additional seismic demand induced by surface waves. Based on relevant bridge pylon engineering demand parameters, four damage states are defined (slight, moderate, extensive, and collapse). This study allows quantifying the shift in a reference fragility curve (defined in terms of body waves only) for each damage state due to the incidence of Rayleigh waves.

Keywords: bridge pylons; vulnerability assessment; fragility analysis; surface waves.

1. Introduction

Even though it is widely recognized that surfaces waves at the edges of sedimentary basins significantly contribute to strong ground motions (Joyner, 2000) (Meza Fajardo et al., 2015), their effects on long-period infrastructures such as liquid storage tanks, tall buildings, and long bridges are still not widely studied. Several research studies have been conducted to assess the response of these modern large-scale infrastructures to strong ground motions (Liu et al., 2021). However, the direct effect of surface waves (in particular, Rayleigh waves) on their seismic response has not been explicitly assessed. A few research studies have suggested a decomposition of strong ground motions into a body wave and a surface wave component and have then quantified the effect of the surface wave component on high-rise buildings (Meza Fajardo et al., 2018) (Meza Fajardo et al., 2019), and bridge piers (Chatzigogos et al., 2020) (Perraud et al., 2022).

Understanding and quantifying the contribution of Rayleigh waves on the seismic response of long-period structures involves some basic steps. In references (Meza Fajardo et al., 2019) (Chatzigogos et al., 2020) (Perraud et al., 2022), the following methodology is implemented: 1) Identification and extraction of Rayleigh waves component from recorded ground motions. 2) Estimation of the seismic response of the analyzed structure subjected to ground motion with and without Rayleigh waves through, for example, time history analyses. 3) Estimation of response amplification associated with the incidence of Rayleigh waves for a number of relevant Engineering Demand Parameters (EDPs) according to the context of application.

Studies on high rise buildings (Meza Fajardo et al., 2019) and bridge pylons (Perraud et al., 2022) highlight maximum response amplifications of about 2 or 3 for linear analyses. For nonlinear analyses, response amplifications can reach up to an order of magnitude (~10) for certain signals and certain relevant engineering demand parameters (EDPs) (see also Perraud et al., 2021).

In the continuation of (Perraud et al., 2022) works on bridge pylons, the present study evaluates the effects of Rayleigh waves on the exceedance probability to damage thresholds for various levels of ground shaking. The conditional probability, also called seismic fragility, is a primary indicator in seismic safety assessment procedures. Thus, in this work, we perform a fragility analysis to gather the results of all possible single-performance scenarios in a continuous function. The distribution is measured by the probability distribution function (PDF) of a chosen engineering demand parameter (EDP) for an intensity measure (IM) of the characteristic ground motion: **P**(EDP—IM).

The fragility assessment is conducted on the basis of transient analyses performed on eight bridge pylon models. The analyses are implemented in an IDA framework (Vamvatsikos et al., 2002) with two distinct loading cases: (i) signals without surface waves and (ii) signals with surfaces waves. The influence of long-period ground motions on the bridge pylon response is quantified by estimating the ratio between the areas of the fragility curves for cases (ii) and (i) pertaining to a given damage state. These studies will provide further insight as of how to incorporate the effects of surface waves on structural vulnerability and applied seismic design.

2. Long period ground motions

The ground motions used in this study consist of 12 natural seismic records from four earthquake events; Niigata-ken Chuetsu (2004), El Mayor-Cucapah (2010), Chi-Chi aftershock (1999), and Tohoku (2011) (see Appendix 1). The records were obtained from national databases and their Rayleigh wave component was extracted through a time-frequency procedure based on the normalized inner product (polarization filtering) developed by (Meza Fajardo et al., 2015) Intensity measures of these records, such as peak ground acceleration (PGA), peak ground velocity (PGV), peak ground displacement (PGV), Arias intensity (I_A), cumulative absolute velocity (CAV), and effective duration are presented in Appendix 1 for:

a) Case 1: The signal without the Rayleigh waves component
b) Case 2: The total signal, i.e., including the Rayleigh waves component

Fig; 1 gathers the PGA and the 5% damped spectral acceleration values for the selected records. The red color is for the signals obtained after the Rayleigh wave extraction procedure (i.e., for Case 1: without the Rayleigh wave effect), and the blue color provides information about the total signal (Case 2). Note that the strongest ground motion record is the one recorded during the Tohoku event at station TKY018 (PGA=1.73m/s^2). A 20% increase is obtained in PGA in passing from Case 1 to Case 2.

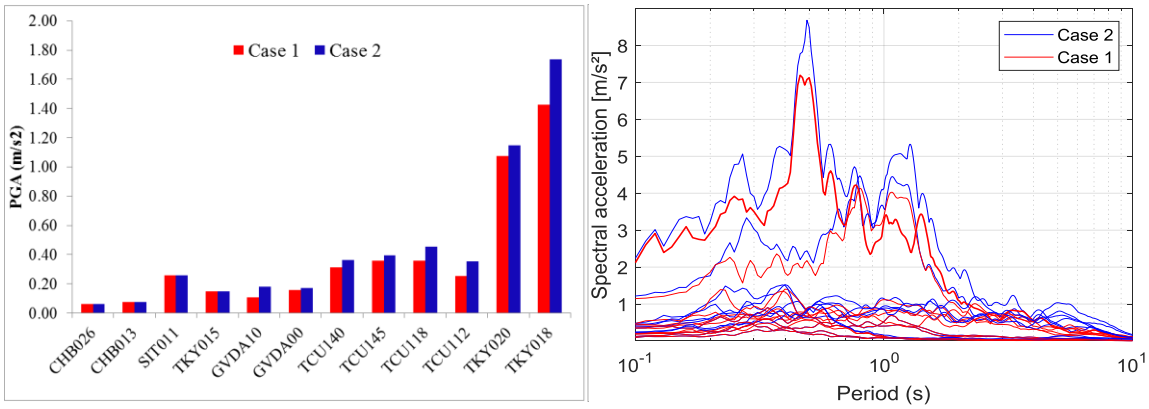

Fig; 1. PGA (Left) and spectral acceleration $S_A(5\%)$ (Right) of the seismic records (Blue) with Rayleigh wave effects and (Red) without Rayleigh wave effects.

The central frequency of the extracted Rayleigh wave components has been reported in (Meza Fajardo et al., 2018) and oscillates between 0.14Hz and 0.20 Hz for the considered signals.

3. Simplified numerical model for bridge pylon

3.1 Main features of the bridge pylon model

The model used to compute the nonlinear response of reinforced concrete bridge pylons is represented in Figure. 1. This model has been developed by (Chatzigogos et al., 2020) under the following assumptions:

a) The pylon is a one-dimensional beam with a uniform circular cross-section discretized using multifiber beam elements. There is no explicit description of concrete and steel in the section, but each fiber has a simplified nonlinear elastoplastic constitutive law that allows obtaining the global yield moment of the section.
b) Each node has three degrees of freedom, two translations and one rotation: $u_x, u_y,$ and θ_z.
c) The pylon supports a portion of the deck at the top end. A local spring-dashpot element ensures the deck-pier connection. At the bottom end, assuming that the foundation system is a shallow foundation, a lumped mass is applied on the first pier node, and a nonlinear foundation macroelement (Chatzigogos et al., 2011) is placed between a control point and the first pier node to reproduce some nonlinear behavior of soil-foundation system under earthquake action (uplift, sliding, soil plasticity).

Further details on the mechanical characteristics of the pylon models, foundations, and soils can be found in (Chatzigogos et al., 2011) or (Perraud et al., 2022).

3.2. Studied configurations

In total, eight pylon configurations are studied with heights: 21m, 30m, 40m, 50m, and 60m. Two foundation sizes are considered for the first three pylons. The pylon properties are presented in Table 1. Pylon diameter is D_p = 3m for all studied cases. Footing width is B_{f1} = 7m for small foundation configurations (S) and B_{f2} = 11m for large foundation

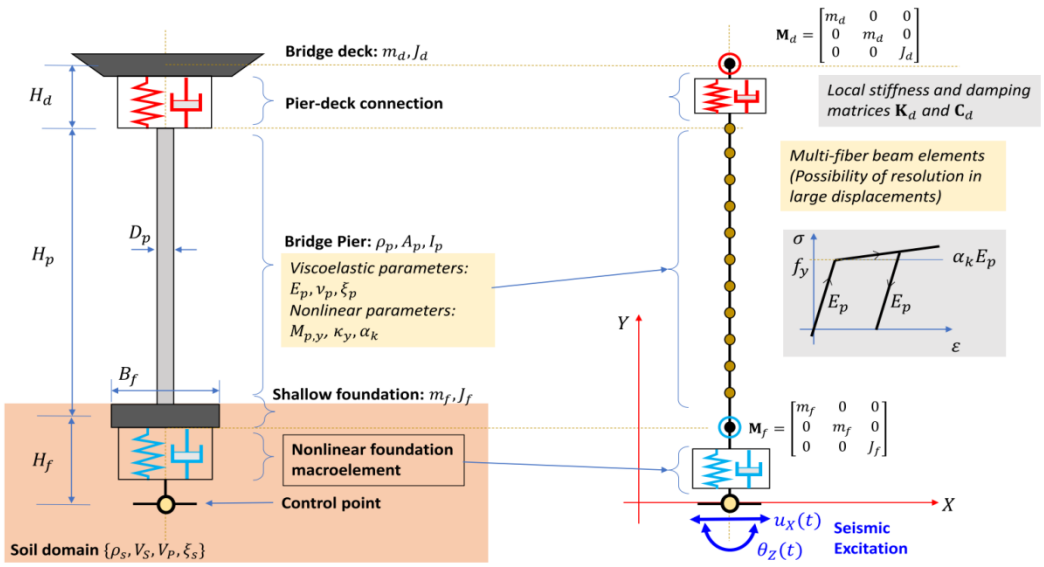

Fig 2. Bridge pylon simplified model (Chatzigogos et al., 2020).

configurations (L). The longitudinal steel ratio of the base section is 1.10%. The studied configurations are summarized in Table 2.

.

Table 1. Parameters of the pylons

Parameter		Unit	P21	P30	P40	P50	P60
Pier height	H_p	[m]	21.0	30.0	40.0	50.0	60.0
Pier section diameter	D_p	[m]	3.0	3.0	3.0	3.0	3.0
Mass density of the bridge pier	ρ_p	[t/m^3]	2.5	2.5	2.5	2.5	2.5
Mass of the deck	m_d	[t]	1200	1200	1200	1200	1200
Moment of inertia of the deck	J_d	[tm²]	23400	23400	23400	23400	23400
Young modulus of pier	E_p	[MPa]	30000	30000	30000	30000	30000
Basic damping ratio of pier	ξ_p	[%]	5.0	5.0	5.0	5.0	5.0
Equivalent yield stress of pier fibers	f_y	[MPa]	16.22	16.22	16.22	16.22	16.22
Hardening parameter for pier fibers	α_k	[MPa]	0.001	0.001	0.001	0.001	0.001
Fundamental period (fixed-base conditions)	T_p	[sec]	1.206	2.036	3.149	4.445	5.914
Total weight of bridge pier	W_{tc}	[MN]	15.41	16.97	18.71	20.44	22.17

Table 2. Studied configurations

	P21	P30	P40	P50	P60
Small foundation (Bf= 7m)	X	X	X	-	-
Large foundation (Bf= 11m)	X	X	X	X	X

4. Nonlinear dynamic analyses

Calculation of seismic fragility requires a wide-range assessment of nonlinear structural response at multiple levels of intensity. Incursion on nonlinear range is essential for

defining fragilities for damage levels from moderate and beyond. Thus, a strategy based on incremental dynamic analyses (IDA) (Vamvatsikos et al, 2002) has been adopted for obtaining a set of nonlinear analyses that adequately describe the possible nonlinear structural states up to a collapse damage level.

4.1 Definition of engineering demand parameters (EDPs)

There are different EDPs (such as drift, displacement ductility, and curvature ductility) that can characterize the reinforced concrete pier behavior. Special attention must be given to the selection of EDPs according to the structure typology and the implemented modeling technique (Chen et al, 2019). The selected EDPs are used for the definition of the damage limit states for an a posteriori construction of fragility curves. In this study, three relevant EDPs are chosen to analyze the seismic response of the studied pylon configurations:

- The curvature ductility ratio (CDR) at the base of the pylon which is defined as the maximum reached curvature $\boldsymbol{\kappa(t)}$ divided by the curvature at first yielding of the steel reinforcing bar and expressed as:

$$\mathrm{CDR} = \max\left(\frac{\kappa(t)}{\kappa_y}\right) \quad (1)$$

- The maximum total drift (MTD) which is defined as the top displacement due to the translation or/and rotation of the foundation and due to the pier bending.
- The foundation settlement (FS) measures the vertical displacement of the superstructure due to the partial loss of bearing capacity of the soil.

4.2 Incremental dynamic analysis (IDA) curves

The results of IDA analyses of the pylons have been reported in (Perraud et al., 2022). The original natural seismic records were amplified with a scale factor (SF) to cover a wide range of signal intensities and develop some nonlinearities (uplift, sliding, soil plasticity, superstructure plasticity). Analyses have been performed for loading Cases 1 and 2 as defined in section 2. Five non-unique scale factors were used to fit specific IM values. In this case, PGV is chosen as the most relevant IM (see discussion in (Perraud et al., 2022) and similar studies (Wei et al., 2020). The seismic records for Case 1 are scaled to PGV values of 0.2, 0.4, 0.6, 0.8 and 1.0 m/s. The corresponding signal in Case 2 is amplified by the same SF as used for Case 1. In total, 960 transient analyses have been performed (8 pylons × 24 seismic signals × 5 scale factors). All nonlinear analyses were run in the finite element platform (Code Aster, 2017). The IDA curves obtained from these analyses are presented in Figs. 3 and 4 for pylons P30S and P30L, respectively. These IDA curves plot the maximum response of the structure as a function of the peak ground velocity (PGV) of the scaled signal. Each line represents a specific ground motion. Significant demands are exhibited in both P30S and P30L for Case 2 (comprising Rayleigh waves). Foundation size determines the location of nonlinear response: in the pylon superstructure (P30L) or in the foundation (P30S). Nonlinear response of pylons founded on large foundations is localized on the piers, governed by large top displacements and significant ductility demands. For pylon configurations with small foundation, large top displacements are also observed but are associated with large foundation rotation. In this case, the nonlinear response is governed by important foundation settlements/rotation, and the pier response remains in the linear elastic range. Depending on foundation size and the subsequent nonlinear response mechanism, fragility curves will be generated using the relevant EDP.

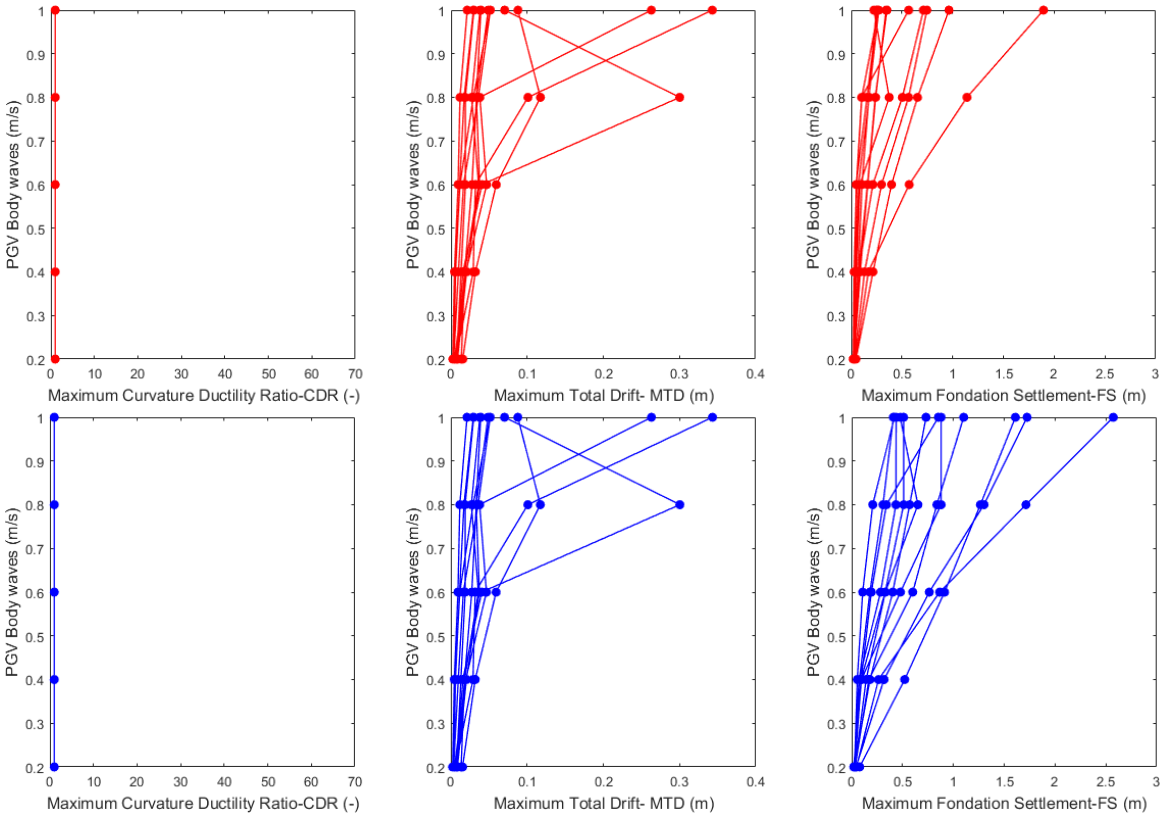

(i) (ii) (iii)

Fig. 3. IDA curves obtained for P30S. In red, for the seismic loading Case 1. In blue, for the seismic loading Case 2: (i) curvature ductility ratio (CDR), (ii) maximum total drift in m (MTD), (iii) maximum foundation settlement in m (FS).

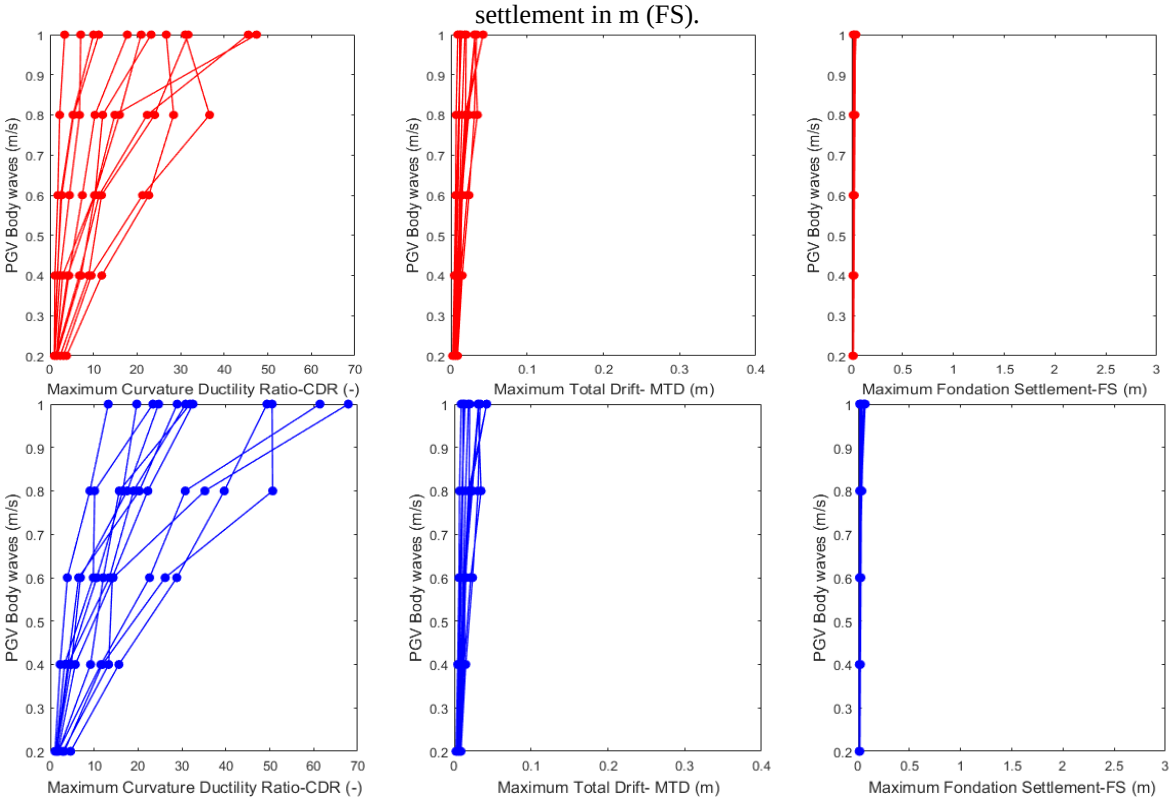

(i) (ii) (iii)

Fig. 4. IDA curves obtained for P30L. In red, for the seismic loading Case 1. In blue, for the seismic loading Case 2: (i) curvature ductility ratio (CDR), (ii) maximum total drift in m (MTD), (iii) maximum foundation settlement in m (FS).

5. Methodology for fragility calculation

Numerous strategies are available in the literature for the construction of analytical fragility curves: moments approximation (e.g., Ibarra et al., 2005), maximum likelihood formulations (Backer, 2015), or regression techniques (e.g., Cornell et al., 2002 and Nielson, 2005). Each method can produce different fragility curves for a given dataset of structural response and one needs to use the most adapted method depending on the available data. In this study, fragility curves are obtained using the least squared regression procedure (LS) (Cornell et al., 2002). As we search to compare the fragility functions produced by the data obtained from two sets of different seismic demands (Case 1 and Case 2), we need to use the data without any binary prejudgment about the damage limit exceedance (exceeded/no exceeded). This is an element that is usually required in the maximum likelihood method. Furthermore, the LS approach can provide a robust relationship between EDP and IM with few data points. However, as verified in previous studies (e.g., Shome et al., 2000), LS regression can be problematic when developing near-collapse or collapse fragility curves, since the results at these stages depend on the reliability of the data (structure modeling technique, nonlinear constitutive laws, loading factors, or ground motion records). For our purposes, this last problem may be considered minor as the main focus of this study is to highlight the differences in fragility with and without the consideration of Rayleigh waves.
Outliers may also significantly affect the fragility curves obtained from LS. Thus, to decrease the influence of outliers present on the piece regressions over the different damage levels, we perform the regression over the whole IM range (from 0.2 m/s to 1.0 m/s).

5.1 Definition of damage states

Results from IDA show that the nonlinear response of the bridge pylons, which develop an inelastic response on the pier, can be described by curvature ductility ratio (CDR) or the maximum total drift (MTD). In contrast, the response of pylons developing nonlinear response on the foundation is better assessed via foundation settlement (FS). Four discrete damage states for the pylons have been adopted following HAZUS-MH (FEMA, 2003) definitions in terms of experimental responses and the considered EDPs:

- *Slight Damage*: minor cracking, minor spalling at pier. Slight vertical displacement of the foundation.
- *Moderate Damage*: moderate cracking and spalling of pier, cracked shear keys or bent bolts of connection, moderate settlement.
- *Extensive Damage*: pier degrading, major settlement.
- *Collapse*: pier collapse or foundation failure.

The literature establishes admissible limit states of concrete piers similar to those of this study in terms of curvature ductility (CDR) with values of 1.0, 2.0, 4.0, and 7.0 for slight, moderate, extensive, and collapse, respectively (Pitilakis et al., 2014) (Choi et al., 2004). Slight damage limits in isolated foundation settlements, FS, by order of 0.05m or differential settlement between supports of 0.02m are proposed in SYNER-G (Pitilakis et al., 2014) used for roadway and railway components. In terms of drift ratios, (Li et al., 2013) proposes the following limit states: 1.45%, 2.46%, 4.30%, and 6.90%, which correspond to yield, cracking, spalling, and reinforcement buckling, respectively. Table 3 summarizes the adopted demand thresholds for the considered damage states in this study.

Table 3. Damage state limits for the tested bridge pylons

EDP	Units	Slight	Moderate	Extensive	Collapse
Curvature Ductility Ratio-CDR	(-)	1.00	2.00	4.00	7.00
Foundation Settlement-FS	(m)	0.02	0.08	0.22	0.70
Maximum Total Drift-MTD / H_p	(%)	1.45	2.46	4.30	6.90

5.2 Least-squares (LS) regression procedure

Once the damage state limits are defined, we derive fragility curves by applying the least-squares regression procedure (or power-law approximation) commonly implemented in seismic fragility analysis (e.g., Cornell et al., 2002 and Nielson, 2005). The fragility function is then defined as the conditional probability that gives the likelihood that a structure seismic demand, or engineering demand parameter (EDP), meets or exceeds a specific level of damage (D) under a specific ground motion intensity measure (IM). The probability of exceedance can be written as:

$$fc(IM; D) = P(EDP \geq D|IM) = \phi\left(\frac{ln\left(S_{EDP_i}/S_D\right)}{\beta}\right) \quad (2)$$

where $\phi[.]$ is the cumulative distribution function of the standard normal distribution. S_{EDP} and S_D are the median values of the demand and capacity, respectively. β_{EDP} and β_D are the logarithmic standard deviations defined by:

$$\beta = \sqrt{\beta_{(D|\mathrm{IM})}{}^2 + \beta_D^2} \quad (3)$$

$$\beta_D = \sqrt{\ln\left(1 - COV^2\right)} \quad (4)$$

$$\beta_{(D|\mathrm{IM})} = \sqrt{\sum_{i=1}^{N}(\ln \mathrm{EDP}_i - \ln S_{\mathrm{EDP}})^2/N - 2} \quad (5)$$

where N is the number of ground motions. EDP_i is the peak value of the seismic response demand under the i-th ground motion. COV is the variation coefficient of the component capacity. The adopted value of COV is 0.25 for the slightly and moderately damaged states, and 0.5 for the severely and completely damaged states (Nielson, 2005). Fig. 5 presents the results of the probabilistic seismic demand model in terms of curvature ductility ratio (CDR) for P40L under the two loading cases; Case 1 and Case 2.

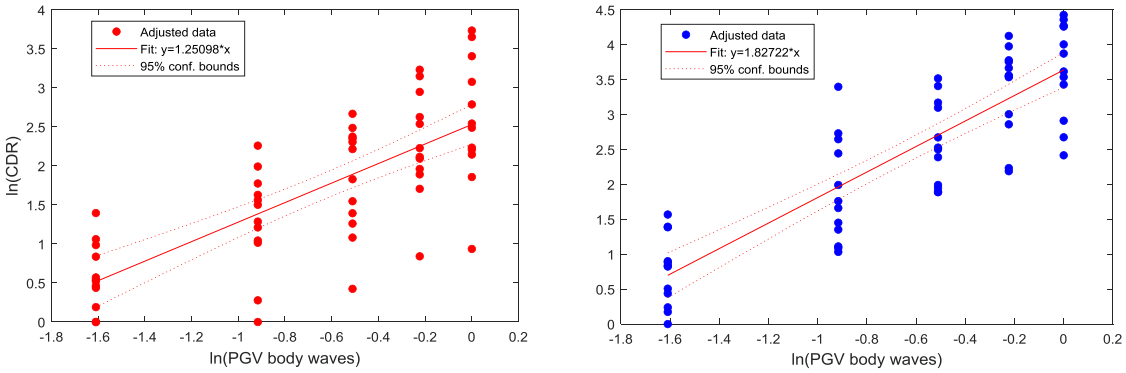

Fig. 5. Regression of the probabilistic seismic demand model of P40L (in terms of CDR) for Case 1 (Left) and Case 2 (Right).

The least-squares regression procedure entails the following steps:

a) Computation of ln(IM) and ln(EDP) (Fig. 5).
b) Define damage state limits (D) that represent the median demand values S_D with its associated dispersion parameter β_D (Equation (4))

c) Perform the regression of the data to estimate the coefficients a and b given by the intercept and slope, respectively. Parameters a and b are calculated as:

$$S_{\mathrm{EDP}} = a\mathrm{IM}^b \text{ and } \ln(\mathrm{EDP}) = \ln a + b \ln \mathrm{IM} \quad (6)$$

$$a = e^{\frac{(\sum y - b \sum x)}{N}} \text{ and } b = \frac{N\sum xy - \sum x \sum y}{N \sum (x^2) - (\sum x)^2} \quad (7)$$

where $x = \ln(\mathrm{IM})\,; y = \ln(\mathrm{EDP})$

d) Compute the median $\theta_{\mathrm{IM}} = \sqrt[b]{S_D/a}$ and the dispersion parameter $\beta_{(D|IM)}$ (Equation (5)).

e) With S_D and β, generate the fitting log-normal distribution function (Equation(2)).

5.3 Fragility curves of bridge pylons

From the previously described procedure, we generate the fragility curves for each pylon with three EDPs: the CDR, MTD, and FS. The parameters of the log-normal distribution in terms of medians and standard deviations are given in Tables 4 and 5 for each pylon and for Case 1 and 2, respectively. Fig. 6 provides the fragility curves for all pylons, for each damage level and for Case 1. Each color line represents a different pylon. All the EDPs have been combined, plotting the most critical case for each pylon (that is, the fragility curve with the smallest median value). For example, for pylons with large foundations, CDR controls the fragility at all the damage limit states. The fragility curves show that the peak ground velocity for a 50% probability of exceeding slight damage ranges from approximately 0.1 to 0.2 m/s for the eight pylon configurations. The pylons with large foundations appear to be the more fragile in all damage states, especially the more severe ones. It is seen that for the pylons on large foundations, there is a 50% probability of exceedance at lower values of PGV than those on small foundations. One should recall that the selected damage thresholds and the modeling technique strongly influence these results. Different conclusions could be obtained if, for instance, only the MTD was taken as the main EPD for the pylons with large foundations.

Fig. 7 shows the fragility curves of P21L,S and P40L,S as a function of PGV of body waves (exempted of the Rayleigh wave component) obtained for the simulations without the effects of surface waves in red (Case1) and with the effects of surface waves in blue (Case 2).

A simplified strategy to compare the fragility curves at each damage limit state is by means of the relative difference of the median between the curves $\Delta\theta_r = (\theta_1 - \theta_2)/\theta_1$. Table 6 (a) presents $\Delta\theta_r$ values. A positive $\Delta\theta_r$ means that the bridge pylon is more vulnerable to Rayleigh waves and a null or negative $\Delta\theta_r$ means that the bridge pylon is not affected by the presence of Rayleigh waves. For the tested pylons, $\Delta\theta_r$ reaches almost 60% at slight damage states and values around 40% at collapse. In the green – red scale, the light green and the strong red colors represent the lowest and the highest relative difference, respectively. This representation helps to qualitatively show that the fragility of Rayleigh waves increases with the damage level and the length of the pylon.

Another simplified strategy to compare the fragilities with or without the Rayleigh wave effects is to compute the ratio between both fragility curve areas A_i through the amplification factor A_f defined in Equation (8). The fragility curve area is bounded by the PGV values at probabilities of exceedance of 0.05 and 0.95. These bounds can be varied to values of interest. The values of A_f for each pylon are given in Table 6.

$$A_i = \int_{\mathrm{PGV}_{min}}^{\mathrm{PGV}_{max}} fc_i(\theta_i, \beta_i)\, d\mathrm{PGV}, \quad A_f = \frac{A_2}{A_1} \quad (8)$$

where,

$\mathrm{PGV}_{min} = \min\{\mathrm{PGV}|_{fc_1=0.05};\ \mathrm{PGV}|_{fc_2=0.05}\}$, $\mathrm{PGV}_{max} = \max\{\mathrm{PGV}|_{fc_1=0.95};\ \mathrm{PGV}|_{fc_2=0.95}\}$

Main important observations can be listed with the help of Tables 4, 5, and 6.

- For all the tested pylons, fragility curves including Rayleigh wave effects are shifted to the left at 50% exceedance probability for all damage states. That is, the defined damage limit states are exceeded at lower PGV values than without the presence of Rayleigh waves.
- Pylons of 21m, 30m, and 40m high with large foundations are less vulnerable than pylons of 50 m and 60m to Rayleigh wave components for all damage states. For slight damage state, the fragility curves for both Case 1 and 2 almost coincide. However, for the pylons with small foundations, the vulnerability can significantly increase for severe damage levels, namely extensive and collapse.
- In general, the exceedance probability at a damage state seems to increase with the pylon height; this is consistent with the results plotted in Fig. 3 and Fig. 4.

The intersections between fragility curves indicate that both loading Cases 1 and 2 lead to identical seismic demands at the intersection PGV values. This would be better appreciated under the superposition of the regressions for Case 1 and 2 in a representation similar to Fig. 5.

Table 4. Parameters of fragility curves for bridge pylon limit state (Case 1)

Pylons	Slight		Moderate		Extensive		Collapse	
	Median (m/s)	β_{IM}	Median (m/s)	β_{IM}	Median (m/s)	β_{IM}	Median (m/s)	β_{IM}
P21L	0.15	0.62	0.26	0.62	0.42	0.62	0.63	0.62
P21S	0.17	0.46	0.40	0.46	0.74	0.46	1.52	0.46
P30L	0.15	0.73	0.24	0.73	0.38	0.73	0.56	0.73
P30S	0.18	0.67	0.40	0.67	0.72	0.67	1.41	0.67
P40L	0.13	0.65	0.23	0.65	0.40	0.65	0.63	0.65
P40S	0.18	0.80	0.38	0.80	0.66	0.80	1.23	0.80
P50L	0.15	0.74	0.25	0.74	0.41	0.74	0.60	0.74
P60L	0.16	0.58	0.25	0.58	0.39	0.58	0.56	0.58

Table 5. Parameters of fragility curves for bridge pylon limit state (Case 2)

Pylon	Slight		Moderate		Extensive		Collapse	
	Median (m/s)	β_{IM}	Median (m/s)	β_{IM}	Median (m/s)	β_{IM}	Median (m/s)	β_{IM}
P21L	0.15	0.51	0.23	0.51	0.36	0.51	0.50	0.51
P21S	0.16	0.56	0.33	0.56	0.56	0.56	1.02	0.56
P30L	0.14	0.53	0.21	0.53	0.31	0.53	0.43	0.53
P30S	0.16	0.60	0.30	0.60	0.50	0.60	0.87	0.60
P40L	0.14	0.63	0.20	0.63	0.29	0.63	0.40	0.63
P40S	0.13	0.78	0.26	0.78	0.43	0.78	0.77	0.78
P50L	0.08	0.78	0.13	0.78	0.22	0.78	0.32	0.78
P60L	0.06	0.70	0.11	0.70	0.20	0.70	0.32	0.70

Table 6. Comparison between fragility curves with and without the Rayleigh wave effects through (a) the relative median difference $\Delta\theta_r$ and (b) the amplification factor computed with Equation (8)

Pylon	Slight	Moderate	Extensive	Collapse
P21L	3%	10%	16%	20%
P21S	8%	19%	25%	33%
P30L	6%	13%	19%	23%
P30S	13%	24%	31%	38%
P40L	-3%	13%	27%	37%
P40S	27%	31%	34%	37%
P50L	48%	47%	47%	46%
P60L	59%	54%	48%	44%

(a)

Pylon	Slight	Moderate	Extensive	Collapse
P21L	1.05	1.10	1.14	1.18
P21S	1.04	1.15	1.22	1.30
P30L	1.09	1.13	1.16	1.19
P30S	1.10	1.17	1.22	1.27
P40L	1.00	1.09	1.18	1.25
P40S	1.14	1.16	1.18	1.20
P50L	1.27	1.27	1.26	1.26
P60L	1.45	1.40	1.35	1.31

(b)

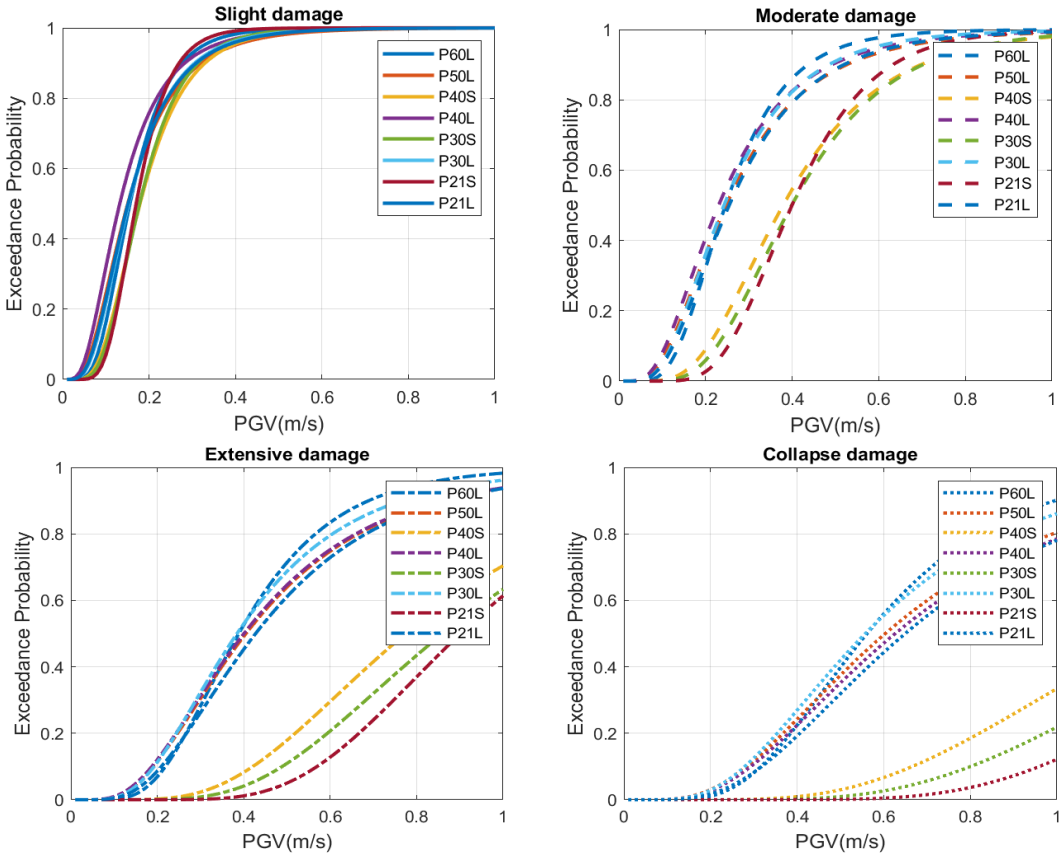

Fig. 6. Fragility curves of Case 1 for all pylons and damage state limits.

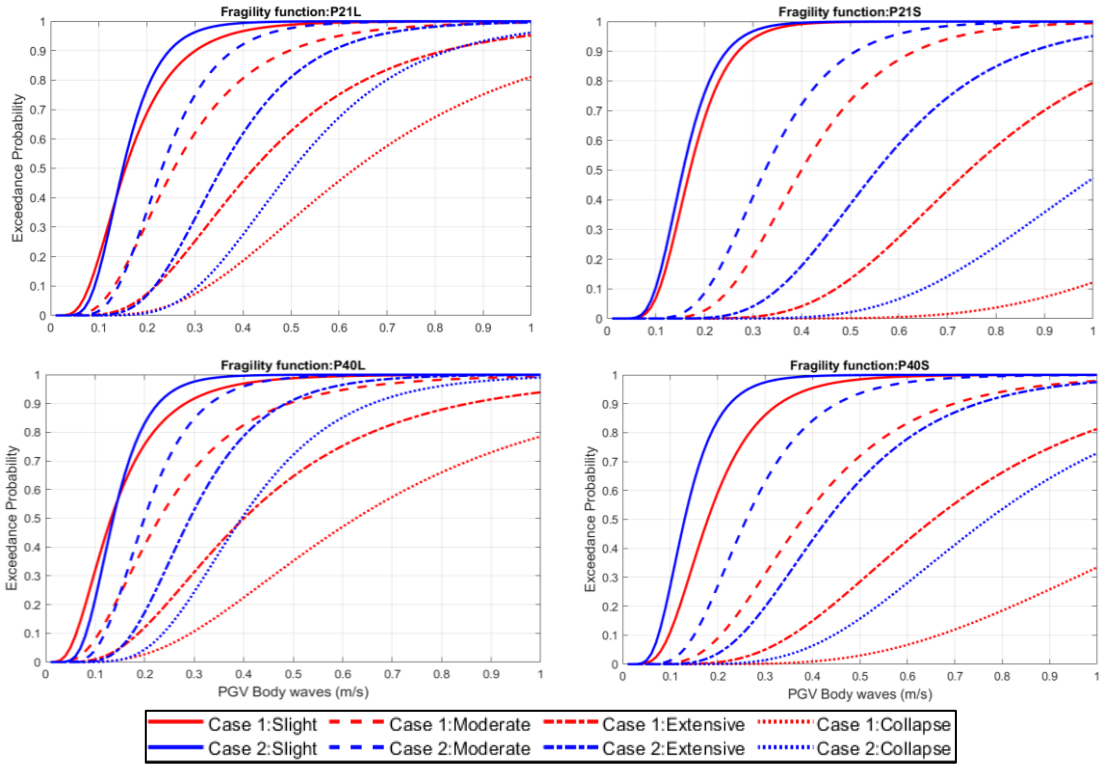

Fig. 7. Comparison of fragility curves for Case 1 and Case 2 in each damage state for P21L, P21S, P40L, and P40S.

6. Conclusions and perspectives

In this paper, we have generated fragility curves for multiple pylon configurations based on the nonlinear results performed in (Chatzigogos et al., 2020) (Perraud et al., 2022). This paper has proposed a strategy to quantify the shift and the amplification in fragility curve for each damage state because of the presence of Rayleigh waves. We observed that an increase in the probability of exceeding a damage limit at a given PGV is obtained for all pylons when the Rayleigh wave effects are taking into account. In agreement with previous results, the fragility study performed in this work shows that pylons of 50m and 60m height, and pylons with short foundations are the most fragile to Rayleigh wave effects. Significant fragility shifts are observed for moderate and severe damage states.

Acknowledgements

This research work has received funding from the French National Research Project ANR MODULATE (2018 - 2022). More details and updates on ANR MODULATE can be accessed through the project website: https://modulate.brgm.fr

References

- Backer J W (2015). Efficient analytical fragility function fitting using dynamic structural analysis. *31*(1), 579-599.
- Chatzigogos C, Figin I R, Pecker A, Salençon J (2011). A macroelement formulation for shallow foundations on cohesive and frictional soils. *International Journal for Numerical and Analytical Methods in Geomechanics, 35*, 902-931.
- Chatzigogos C, Meza Fajardo K, Papageorgiou A (2020). Nonlinear response of bridge pylons to surface wave passage. *Proceedings of 17WCEE.* Sendai, Japan, September 13-18, 2020.
- Choi E, DesRoches R., Nielson B (2004). Seismic fragility of typical bridges in moderate seismic zones. *26*(2), 187-199.
- Code Aster (2017). *Analysis of Structures and Thermomechanics for Studies and Research.* Consulté le 2022, sur https://www.code-aster.org
- Cornell A, Jalayer F, Hamburger R O (2002). Probabilistic Basis for 2000 SAC Federal Emergency Management Agency Steel Moment Frame Guidelines. *128*(24), 526-532.
- FEMA (2003). *HAZUS-MH MR1: Technical Manual* (Vol. Vol. Earthquake Model). Washington DC: Federal Emergency Management Agency,.
- Ibarra L F, Helmut K (2005). *Global collapse of frame structures under seismic.* Stanford, CA: tHE John A. Blume Earthquake Engineering Center, Department of Civil Engineering, Stanford University.
- Joyner W B (2000). Strong motion from surface waves in deep sedimentary basins. *Bulletin of the Seismological Society of America, 90*(6B), S95--S112.
- Li J, Spencer B, Elnashai A (2013). Bayesian Updating of Fragility Functions Using Hybrid Simulation. *139*(7).
- Liu S, Jiang Y, Li M, Xin J, Peng L (2021). Long period ground motion simulation and its application to the seismic design of high-rise buildings. *Soil Dynamics and Earthquake Engineering, 143*, 106619.
- Meza Fajardo K C, Aochi H, Papageorgiou A (2021). Comparative analysis of Rayleigh and Love waves detected propagating in the Nobi and Kanto basins during the 2004-, 2007- Chuetsu and 2011 Tohoku earthquakes. *143*(ISSN 0267-7261), 106606.
- Meza Fajardo K C, Papageorgiou A (2018). Response of tall buildings to base rocking induced by Rayleigh waves. *Earthquake Engineering and Structural Dynamics, 47*, 1755-1773.
- Meza Fajardo K C, Papageorgiou A (2019). Ductility demands of tall buildings subjected to base rocking induced by Rayleigh waves. *Earthquake Engineering and Structural Dynamics*, 1-21.
- Meza Fajardo K C, Papageorgiou A, Semblat J-F (2015). Identification and extraction of surface waves from three-component seismograms based on the Normalized Inner Product. *Bulletin of the Seismological Society of America, 105*, 210-229.
- Nielson B G (2005). *Analytical fragility curves for highway bridges in moderate seismic zones.* Georgia Institute of Technology.

- Perraud Y, Chatzigogos C, Meza Fajardo K C (2021). *Seismic performance of long period large-scale infrastractures. Evaluation of structural response with surrogate models.* France: French National Reseach. Project - ANR modulate.
- Perraud Y, Chatzigogos C, Meza Farjardo K, Labbé P (2022). Effect of Rayleigh waves on seismic response of bridge pylons via Incremental Dynamic Analyses. *Soil Dynamics and Earthquake Engineering, 152*.
- Pitilakis K, Crowley H, Kaynia A (2014). *SYNER-G: Typology Definition and Fragility Functions for Physical Elements at Seismic Risk* (Vol. Geotechnical, Geological and Earthquake Engineering, 27). Springer.
- Shome N, Cornell C A (2000). Structural seismic demand analysis: consideration of collapse. *8th ASCE Specialty Conference on Probabilistic Mechanics and Structural Reliability*, pp. 1--6.
- Vamvatsikos D, Cornell C (2002). Incremental dynamic analysis. *Earthquake Engineering and Structural Dynamics, 31*, 491-514.
- Wei B, Hu Z, He X, Jiang L (2020). Evaluation of optimal ground motion intensity measures and seismic fragility analysis of a multi-pylon cable-stayed bridge with super-high piers in Mountainous Areas. *Soil Dynamics and Earthquake Engineering, 129*.

Appendix 1.

Table 7. Earthquake events and seismic records together with the intensity measures for the total signal (with Rayleigh waves) and the body wave signal (without Rayleigh waves)

Record	Earthquake	Niigata-ken Chuetsu				El Mayor-Cucapah		Chi-Chi aftershock 1803				Tohoku	
	Year	**2004**				**2010**		**1999**				**2011**	
	Magnitude	6.80	6.80	6.80	6.80	7.20	7.20	6.20	6.20	6.20	6.20	9.00	9.00
	Depth [km]	300.00	300.00	300.00	300.00	206.70	206.70	60.00	60.00	60.00	60.00	29.00	29.00
	Record Name	**CHB026**	**CHB013**	**SIT011**	**TKY015**	**GVDA10**	**GVDA00**	**TCU140**	**TCU145**	**TCU118**	**TCU112**	**TKY020**	**TKY018**
Case 1: Total signal (with Rayleigh waves)	**PGA [m/s2]**	0.06	0.07	0.26	0.15	0.18	0.17	0.36	0.40	0.45	0.36	1.15	1.73
	PGV [m/s]	0.01	0.01	0.03	0.03	0.03	0.03	0.16	0.14	0.15	0.12	0.25	0.36
	PGD [m]	0.01	0.01	0.02	0.02	0.06	0.04	0.13	0.12	0.10	0.09	0.10	0.10
	I_A [m/s]	0.00	0.00	0.02	0.01	0.01	0.01	0.11	0.09	0.09	0.06	0.97	2.01
	CAV [m/s]	1.56	0.83	2.69	3.17	1.72	1.67	6.35	5.44	4.63	3.63	23.28	32.20
	Effective Duration [s]	243.26	87.94	70.16	157.70	46.01	40.77	58.33	62.01	47.76	43.33	103.32	95.40
Case 2: Body wave component (without Rayleigh waves)	**PGA [m/s2]**	0.06	0.07	0.26	0.15	0.11	0.16	0.31	0.36	0.36	0.25	1.07	1.42
	PGV [m/s]	0.01	0.01	0.03	0.02	0.01	0.01	0.10	0.08	0.11	0.07	0.23	0.29
	PGD [m]	0.01	0.01	0.02	0.02	0.02	0.01	0.08	0.07	0.07	0.06	0.10	0.10
	I_A [m/s]	0.00	0.00	0.02	0.01	0.00	0.01	0.06	0.05	0.06	0.03	0.69	1.23
	CAV [m/s]	1.42	0.78	2.51	2.98	1.36	1.36	4.73	4.06	3.62	2.43	19.01	25.26
	Effective Duration [s]	261.95	81.11	75.97	170.54	78.37	51.56	61.87	64.50	49.39	50.24	96.92	95.08